Bioorganic Chemistry 108 (2021) 104660

Contents lists available at ScienceDirect

Bioorganic Chemistry

journal homepage: www.elsevier.com/locate/bioorg

Influence of core extension and side chain nature in targeting G-quadruplex structures with perylene monoimide derivatives

Natalia Busto [a,*], José García-Calvo [a], José Vicente Cuevas [a], Antonio Herrera [b], Jean-Louis Mergny [c,d,e], Sebastian Pons [b], Tomás Torroba [a], Begoña García [a]

[a] Chemistry Department, University of Burgos, Pza. Misael Bañuelos s/n, 09001 Burgos, Spain
[b] Molecular Biology Institute of Barcelona, IBMB-CSIC, 08028 Barcelona, Spain
[c] ARNA Laboratory, INSERM U1212, CNRS UMR 5320, IECB, University of Bordeaux, F-33600 Pessac, France
[d] Institute of Biophysics, AS CR, v.v.i. Kralovopolska 135, 612 65 Brno, Czech Republic
[e] Laboratoire d'optique et Biosciences, Ecole Polytechnique, CNRS, Inserm, Institut Polytechnique de Paris, Palaiseau, France

ARTICLE INFO

Keywords:
G-quadruplexes
Antiproliferative
Perylenemonoimide
DNA binding

ABSTRACT

A structure–activity relationship (SAR) study in terms of G-quadruplex binding ability and antiproliferative activity of six fluorescent perylenemonoimide (PMIs) derivatives is reported. A positive charge seems to be the key to target G4. This study also reveals the importance of the element substitution in the potential biological activity of PMIs, being the polyethylene glycol (PEG) chains in the *peri* position responsible for their antiproliferative activity. Among them, the cationic **PMI6** with two PEG chains is the most promising compound since its fluorescence is enhanced in the presence of G-quadruplex structures. Moreover, **PMI6** binds to the human telomeric G-quadruplex hTelo with high affinity and displays a high antiproliferative potential towards HeLa (cervical adenocarcinoma), A549 (lung adenocarcinoma) and A2780 (ovarian adenocarcinoma) cells. Its fate can be followed inside cells thanks to its fluorescent properties: the compound is found to accumulate in the mitochondria.

1. Introduction

Apart from the well-known classical double-helix conformation, DNA can adopt a variety of non-canonical secondary conformations such as G-quadruplex (G4) structures. G-quadruplexes have attracted a great deal of attention in the last decades due to their roles in DNA replication, transcription and genome stability [1] and consequently, in some human diseases [2]. G4s result from the stacking of several G-quartets stabilized by monocations, each quartet being formed by four guanines interacting by Hoogsteen Hydrogen bonds [3].

Even if a large number of G-quadruplex binding ligands has been reported [4,5] there is still a need to develop selective G4 stabilizing ligands, to better understand the biological roles of these structures and their potential as therapeutic targets [6,7]. Due to the potential of G-quadruplexes as therapeutic targets [8] and the still limited knowledge of the biological properties of these structures [9], the development of G4 binders has become an important scientific challenge, not only as anticancer[4,5,7,8,10,11] or antiviral agents [12–15] but also as fluorescent probes [8,16,17]. Some common features are recurrent in the design of these drugs, such as the presence of aromatic rings in order to interact with the G-quartets by π- π stacking interactions, positive charges to facilitate the binding by electrostatic interactions with the negative phosphates and side chains with functional groups that enable final stabilization of the whole structure by H-bonding or Van der Waals interactions.

The perylene scaffold turned out to be a very successful starting point for the design of G4 ligands [18–20]; the classical representative, PIPER (*N*,*N*'-bis-(2-(1-piperidino)ethyl)-3,4,9,10-perylenetetracarboxylic acid diimide), not only binds to G4 but also induces G4 formation [21]. The selectivity of perylenediimide derivatives (PDIs) towards G4 over duplexes is modulated by the functionality of the side chains [22,23]. As an example, it has been described that the addition of *N*-cyclic substituents at *bay* positions gives excellent results in terms of G4 selectivity and anticancer activity [24–26]. On the other hand, perylenemonoimides (PMIs) are scarcely reported as G4 ligands. Two perylenemonoimide derivatives have been shown to bind G4 and down-regulate the gene expression of the angiogenic factor VEGF [27]. From them, only one derivative, PM2, has been further reported in G4-related studies

* Corresponding author.
E-mail address: nbusto@ubu.es (N. Busto).

https://doi.org/10.1016/j.bioorg.2021.104660
Received 10 December 2020; Received in revised form 12 January 2021; Accepted 12 January 2021
Available online 28 January 2021

[28,29].

In this context, we present here the G4 binding results of a family of fluorescent perylenemonoimide derivatives decorated at the *peri* position with pyridine or pyrimidine moieties to extend the perylene core and enhance π-stacking with the G-tetrads. In addition, these groups bring a substituted piperazine with hydrophilic tails to improve solubility in aqueous solution and prevent self-aggregation. As hydrophilic tails we selected one or two polyethylene glycol (PEG) side chains, or a biotin residue. Both groups have been frequently used, [30,31] having good cytocompatibility, [20,32] that permits extension of the study of PMI derivatives to fluorescent labeling or live cell imaging. PEG chains are also active players in G4 conformation studies; in this way, the conversion of the two hybrid type topologies of the human telomeric G4 hTelo to a propeller-type form by long PEG tails was described [33]. Other authors attached PEG tails to a known G4 ligand, 3,6-bis(1-methyl-4-vinylpyridinium)carbazole diiodide [BMVC], leading to a conformational change from non-parallel to parallel G4 structures [34]. In our case, the binding ability of six synthesized PMIs towards G-quadruplex structures, their antiproliferative activities, and the biological behavior of the most promising compound have been studied; from them structure–activity relationships (SAR) have been established.

2. Results and discussion

The synthesis of the six perylenemomoimide derivatives started by the Suzuki reaction of the bromoperylenemonoimide **I** with one equivalent of a *N*-Boc protected piperazinyl-pyrimidine(or pyridine)boronic ester (**II-III**) (Scheme 1) and one equivalent of Na_2CO_3, under catalysis by $Pd(PPh_3)_4$ in Tol:BuOH:H_2O (4:1:0.3 v/v), following standard conditions [35–37]. Work-up of the reactions followed by column chromatography of residues afforded the *N*-Boc protected derivatives **IV** and **V** (69–74% yield). Quantitative deprotection of **IV-V** and then acylation or mono/dialkylation (52–92% yield) of the deprotected amine group gave derivatives **PMI1-6** used in this study. In detail, the unsubstituted piperazine-pyridine derivative **PM1** was pegylated to compound **PMI2** and unsubstituted piperazine-pyrimidine derivative **PM3** was biotinylated to **PM4**, mono-pegylated to **PM5** and bis-pegylated to the cationic **PM6**. In these compounds the flat aromatic backbone of the perylenemonoimide central core has been extended by a conjugated pyridine or pyrimidine group. In contrast, the periphery of the compounds has a dual nature: on one side they carry a polar piperazine group with highly hydrophilic diethylene glycol methyl ether pendant groups (or an extended biotin) while on the other side they carry a non-polar bulky 1-adamantylethyl group, suitable for hydrophobic interactions.

2.1. G-quadruplex interaction

The ability of **PMI1-6** to thermally stabilize G4 structures was studied by FRET melting assays. We compared binding to a variety of G-

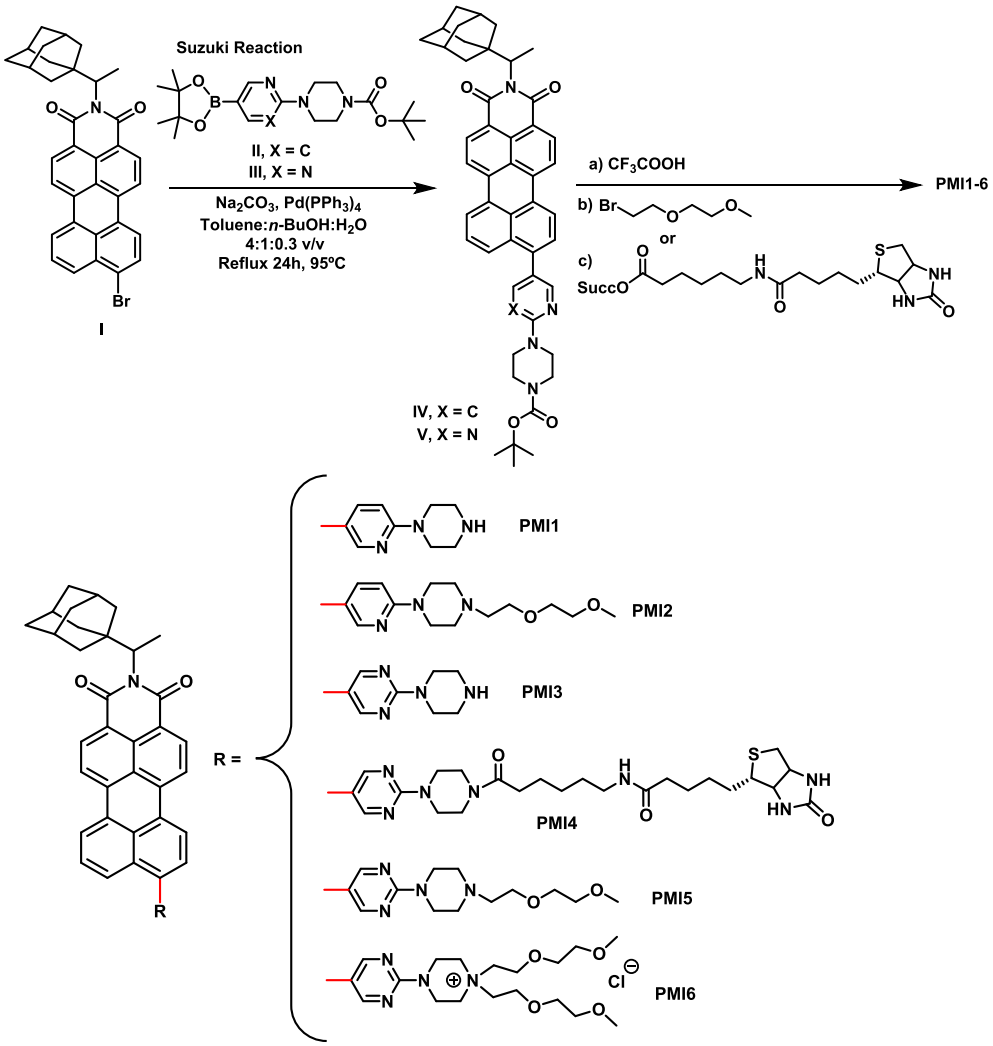

Scheme 1. Synthesis of the six perylenemomoimide derivatives **PMI1-6** used in the study.

quadruplexes, including a parallel RNA (21R) and different conformations of DNA G4: parallel (c-myc, 25ceb), antiparallel (21CTA, TBA, Bom17) and hybrid-type (hTelo) quadruplexes as well as an intramolecular duplex (dX). The radar plot of the ΔTm of various oligonucleotides in the presence of the studied compounds is shown in Fig. 1 and the exact ΔTm values collected in Table S1. **PMI2**, **PMI4** and **PMI5** had little effect on all these DNA structures. On the other hand, **PMI1**, **PMI3** and especially **PMI6** showed very good thermal stabilization values of the quadruplexes. **PMI1** and **PMI3**, being closely related, showed a surprisingly different behavior. **PMI1** had a strong stabilizing effect on the parallel RNA G4 21R and the hybrid G4 hTelo, while **PMI3** showed the highest stabilizing effect on antiparallel G4s. Therefore, the change in one single atom in the structure had a clear effect in the G4 thermal stabilization patterns, according to the FRET melting results. **PMI6** was the most active term of the series, inducing the highest stabilization of G4 structures. The most stabilized G4 was the human telomeric G-quadruplex (hTelo), which predominantly adopts a hybrid-type conformation. The induced thermal stabilization by **PMI1**, **PMI3** and **PMI6** was concentration-dependent (Figure S42). At a fixed PMI/G4 ratio, the highest fluorescence enhancements were obtained in the presence of the parallel G4 c-myc for **PMI1**, the antiparallel G4 21CTA for **PMI3** and the hybrid hTelo for **PMI6**. For **PMI3** and **PMI6**, both bearing pyrimidine, the parallel topologies were the less stabilized G4s. Only **PMI6** had a slight stabilizing effect on the intramolecular duplex.

Topological selectivity currently remains incomplete; if accomplished, it would substantially impact cancer therapy [7]. Thus, taking advantage of the emission properties of the synthesized perylenemomoimide derivatives, additional fluorescence measurements with a parallel (c-myc), an antiparallel (21CTA) and a hybrid (hTelo) G4s were performed (Fig. 2) in order to confirm PMIs' conformational preference. The fluorescence emission of **PMI1**, **PMI3** and **PMI6** increased in the presence of G4 structures, and the magnitude of this increase was correlated with the melting stabilizations reported above: the most thermally stabilized topology is the G4 that produced the highest emission enhancement. Once more, **PMI6** turns to be the most G4-responsive compound.

From these results, we conclude that only **PMI1**, **PMI3** and **PMI6** are able to thermally stabilize G4 structures. According to the reported acid dissociation constant of NH^+ methyl substituted N atom of 1-methyl-4-phenyl-piperazine ($pKa_1 = 7.82 \pm 0.07$) [38] and the calculated pKa for **PMI3**, $pKa = 7.70 \pm 0.69$ (Figure S43), there is an equilibria between the

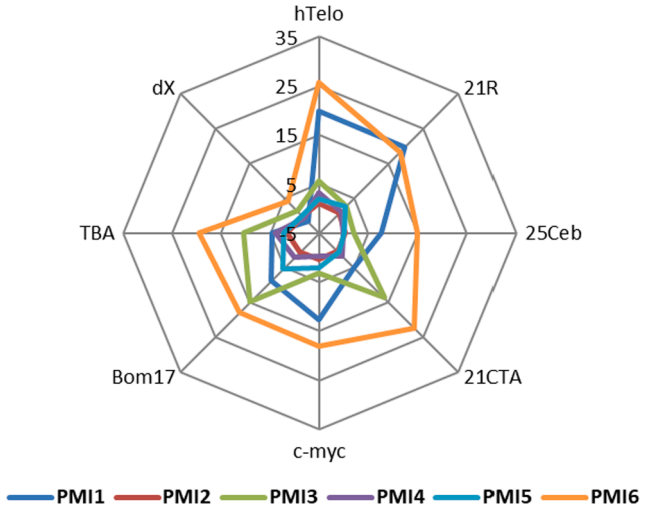

Fig. 1. Radar plot of the ΔTm of various oligonucleotides in the presence of 10 μM of the studied compounds. All fluorescent oligonucleotides were tested at 0.2 μM strand concentration. dX is a control duplex while all other sequences correspond to intramolecular RNA (21R) or DNA (hTelo, 25Ceb, 21CTA, c-myc, Bom17 and TBA) quadruplexes, all labeled with 5′FAM and 3′TAMRA.

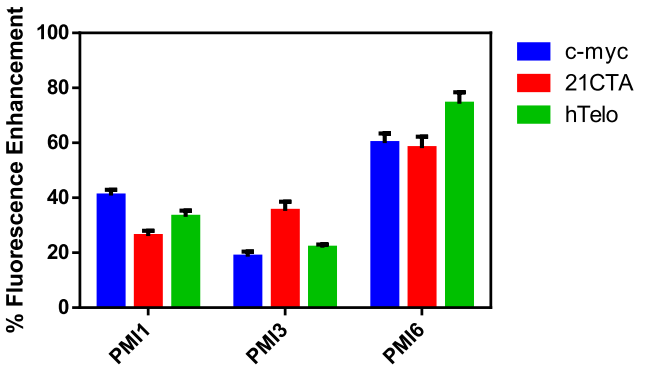

Fig. 2. Fluorescence enhancement of 15 μM of **PMI1**, **PMI3** and **PMI6** in the presence of G-quadruplex structures with different topologies. $\lambda_{exc} = 510$ nm, $C_{PMI}/C_{G4} = 0.1$, I = 0.11 M (90 mM LiCl, 10 mM KCl, 10 mM LiCaC), pH = 7.2 and T = 25 °C.

protonated and non-protonated species in the secondary amino group of **PMI1** and **PMI3**. Thus, the positive charges in **PMI1**, **PMI3** and **PMI6** are essential for the thermal stabilization of G-quadruplex structures. Among them, the cationic **PMI6** with two PEG chains induces the highest G4 thermal stabilization. The action of the side chains of perylenediimide derivatives [23] and other classic scaffolds such as bisindole derivatives [39] in G4 binding modulation has been previously described. Our results confirm the importance of the side chains in the activity of this new family of compounds. Since **PMI6** induces the greatest stabilization of G4s, further studies were conducted to delve into the G4 binding mechanism and to test the biological activity of the new compound in search of potential antiproliferative activity

2.2. *G-quadruplex binding of **PMI6***

FRET Melting Competition Assay: We performed a competition FRET melting assay to properly evaluate the selectivity of **PMI6** for G4 structures over double stranded DNA. It consisted on the evaluation of the variation of ΔTm with and without competitor; in this case, a 15- to 50-fold excess of duplex DNA (ds26, as compared to hTelo) was employed. At 10 μM of the studied compounds, no competition was detected. By contrast, when the concentration of **PMI6** decreased, that is, at 5 μM, a slight variation of the hTelo thermal stabilization ($\Delta\Delta Tm \approx -3°C$) at the highest excess (50 fold) of competitor was observed (Fig. 3).

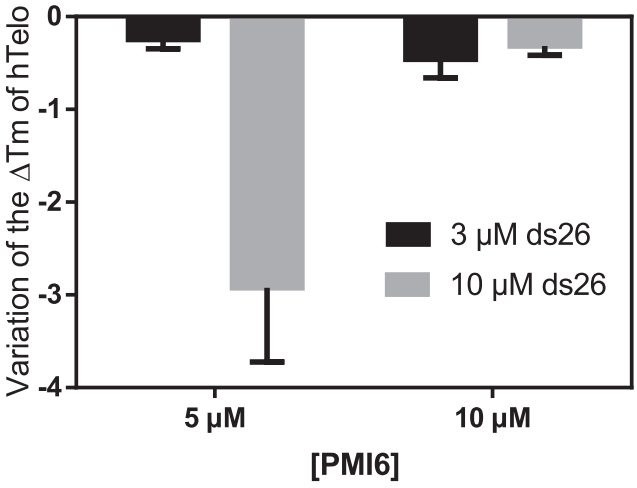

Fig. 3. Variation of hTelo ΔTm ($\Delta Tm_{competitor}$ - $\Delta Tm_{w/o\ competitor}$) induced by 5 and 10 μM of **PMI6** in the presence of different concentrations of competitor (ds26). $C_{hTelo} = 0.2$ μM.

Emission properties study: There are several examples in the literature of G4 binders whose fluorescence is enhanced in the presence of parallel or antiparallel G4s [40–43]. and of fluorophores able to induce a parallel conformation upon binding [44,45] Nevertheless, the number of reported fluorophores that turn-on preferably in the presence of hybrid G4s without affecting the hybrid-type topology is scarce. As **PMI6** is fluorescent (Figure S44), its emission in the presence of various DNA structures was investigated. We monitored the effect of single-stranded (ds17a) or double-stranded DNA (ctDNA), parallel G4 (c-myc), antiparallel G4 (21CTA) and hybrid G4 (hTelo). Interestingly, **PMI6** emission increased substantially in the presence of G-quadruplexes (Fig. 4A), especially hTelo, and the increase was selective with respect to other types of oligonucleotides.

The binding was also confirmed by time-correlated single-photon counting (TCSPC) since the obtained fluorescence lifetimes of **PMI6** significantly increased (by ≈1 ns) in the presence of a 2-fold excess of G4s (Fig. 4B) which may be related to a restriction in the intramolecular rotational diffusion of **PMI6** upon G4 binding [46]. Similar fluorescence lifetimes in the presence of G4 were obtained for other fluorescent G4 binders such as 3,6-bis(1-methyl-2-vinyl-pyridinium)carbazole diiodide (**o-BMVC**) whose differences in lifetimes when bound to dsDNA or G4 enabled its use to visualize G4s in fixed cells by FLIM (fluorescence lifetime imaging microscopy) [47,48]. According to the calculated lifetimes in the presence of parallel, antiparallel and hybrid G4 topologies (Fig. 4B), **PMI6** acts as a generalist probe for all G4 conformations, in contrast with a recently described G4 cationic probe **NBTE** (4,4′,4′′-(nitrilotris(benzene-4,1-diyl))tris(1-ethylpyridin-1-ium) iodide) [49].

Isothermal Titration Calorimetry: Since the largest increase in fluorescence intensity of **PMI6** is observed with hybrid-type G4 (hTelo), and this human telomeric G4 is also the most thermally stabilized, the affinity of **PMI6** for hTelo was further investigated by isothermal calorimetry (ITC) titrations (Fig. 5). The obtained binding isotherm showed a biphasic behavior. Therefore, a "Multiple Binding Sites" model was applied to determine the thermodynamic parameters of the **PMI6** interaction with hTelo; the results are shown in Table 1.

PMI6 binding to hTelo was not a simple process. There were at least two different binding processes, with high binding constants; explicitly, **PMI6** strongly binds hTelo with affinities comparable to Ni-salphen, Ni-bypiridine complexes [50], some terpyridine derivatives [51] and pyridostatin [52]. According to the obtained parameters, both processes are exothermic but the binding of **PMI6** to one of the binding sites (named as 1) is more exothermic than the binding to the other binding site (named as 2). In the light of the obtained T·ΔS values, binding process 1 for **PMI6** interaction is enthalpically driven, whereas the second binding process is mostly entropy driven at 25 °C.

Circular Dichroism measurements: Performed CD titrations showed that no significant conformational change of the hybrid type conformation of hTelo is induced (Figure S45). Apparently, the two short PEG chains do not provide **PMI6** with the ability to induce a

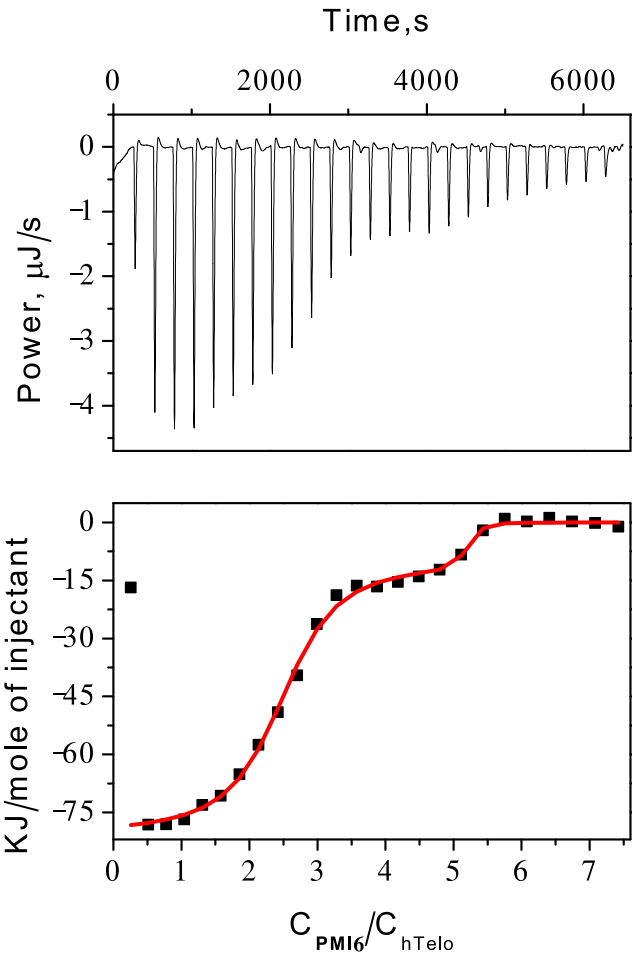

Fig. 5. ITC titration of 39 μM hTelo with **PMI6**.

Table 1
Thermodynamic parameters obtained for the **PMI6**/hTelo interaction by ITC measurements at I = 0.11 M (90 mM LiCl, 10 mM KCl, 10 mM LiCaC), pH = 7.2, T = 25 °C.

10^{-8} × K_1 (M^{-1})	ΔH_1 (kJ·mol^{-1})	-T·ΔS_1 (kJ·mol^{-1})	10^{-7} × K_2 (M^{-1})	ΔH_2 (kJ·mol^{-1})	-T·ΔS_2 (kJmol^{-1})
5.0 ± 1.0	−49.5 ± 1.9	−0.17	1.3 ± 0.9	−6.4 ± 0.8	−34.3

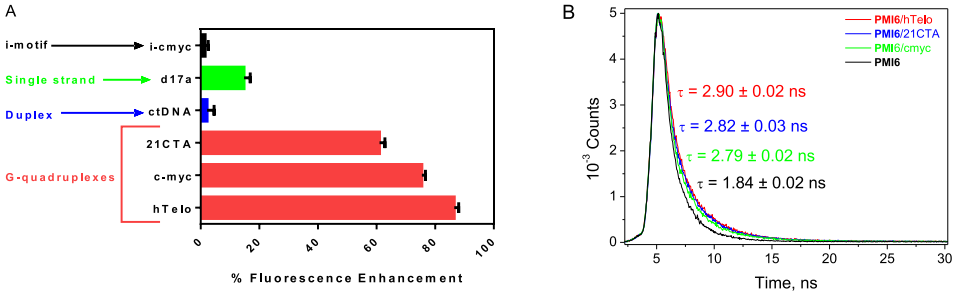

Fig. 4. **(A)** Percentage of fluorescent enhancement of 10 μM of **PMI6** upon addition of various oligonucleotides in different conformations. C_{PMI6} = 10 μM, C_{PMI6}/C_{Oligo} = 0.2, λ_{exc} = 486 nm, I = 0.11 M (90 mM LiCl, 10 mM KCl, 10 mM LiCaC), pH = 7.2 except for i-motif (pH = 5.8) and 25 °C. **(B)** TCSPC decays of 10 μM of **PMI6** in the absence and in the presence of G-quadruplexes. C_{Oligo}/C_{PMI6} = 2, λ_{exc} = 475 nm, I = 0.11 M (90 mM LiCl, 10 mM KCl, 10 mM LiCaC) pH 7.2 and 25 °C.

topological change in hTelo, in contrast with the reported behavior for other G4 ligands with longer attached PEGs. Once substantial conformational changes are discarded, quantum chemical calculations were performed to enlighten the structure of **PMI6**/hTelo complexes.

Theoretical studies: As a first step, a molecular docking study was performed to predict the most stable conformations of the interaction in a 1:1 complex. The lower energy structure from the docking study was then further optimized using the semiempirical GFN2-xTB method (See Experimental Section for details). Following the same procedure, the interaction between hTelo and two units of **PMI6** was then modeled. Thus, the previously optimized 1:1 complex structure was used as one component for a molecular docking study with a second molecule of **PMI6**. The docked structure of lowest energy was further optimized using the semiempirical GFN2-xTB method. The obtained structures can be described as an interaction of the first unit of **PMI6** with hTelo by groove binding (Fig. 6A) through π-stacking interaction between the adenine-9 and the perylene moiety of **PMI6** (See Supporting Information for further details, Figs. S46 – S54). This binding mode differs from the end stacking reported for the first perylene –based G-quadruplex ligand PIPER, in which the perylene core interacts with the terminal G-tetrad by π-π stacking interactions [53,54]. Thus, to corroborate if the used methodology was adequate, the same molecular docking study was carried out with PIPER giving rise to a structure in which PIPER access to the top of the G-tetrad (Fig. S55). Fig. 6B shows the second **PMI6** molecule interacting with the adenine-1 and thymine-20 through the pyrimidine ring and the perylene moiety, respectively. Additional C—H···π interactions between the adamantyl fragment and the perylene moiety of the **PMI6** units can be found, as well as polar interactions between the polyether units and phosphate groups. The pyrimidine group in both cases seems to play a crucial role in the molecular interactions that contribute to the fitting of **PMI6** to hTelo by extending the planar structure and by additional polar and π-stacking interactions. Also, in both cases, the adamantane groups occupy hydrophobic pockets and the bis-pegylated ammonium group present some polar interactions with the external parts of the hTelo structure.

2.3. Biological activity

The cytotoxicity of these perylenemonoimide derivatives was evaluated in tumor cells: HeLa (cervix), A2780 (ovary) and A549 (lung) and in human embryonic kidney cells (HEK293). The obtained half maximal inhibitory concentrations (IC_{50}) after 72 h of exposition are shown in Table 2. From them, it can be deduced that the replacement of the pyridine moiety by a pyrimidine leads to a decrease of the antiproliferative activity. Undoubtedly, the PEG chains played a key role in the cytotoxicity since only PMIs bearing PEG(s), **PMI2**, **PMI5** and **PMI6**, displayed antiproliferative activity and among them, **PMI6** was the most potent antiproliferative PMI. The antiproliferative activity found here is in strong contrast with the expected behavior since PDIs bearing PEG have been described as not cytotoxic at 24 h of exposition in HeLa cells [32].

Table 2
IC_{50} values of the synthesized PMI derivatives in HeLa, A2780, A549 and HEK293 cells after 72 h of exposition.

	HeLa (μM)	A2780 (μM)	A549 (μM)	HEK293 (μM)
PMI1	>40	>40	29.6 ± 2.6	38.6 ± 3.2
PMI2	18.7 ± 1.6	19.1 ± 1.3	23.4 ± 2.1	33.8 ± 1.6
PMI3	>40	>40	>40	>40
PMI4	>40	>40	>40	>40
PMI5	21.4 ± 2.8	>40	35.2 ± 2.5	38.3 ± 3.2
PMI6	4.1 ± 1.0	31.3 ± 2.4	15.7 ± 1.2	>40

At this stage, **PMI6** is the most interesting PMI since its bears two fundamental structural elements: the positive charge that enables G4 interactions and the PEG chains that increase its antiproliferative potential. However, in the light of the antiproliferative results, G4 interaction and cytotoxic activity cannot be straightforwardly correlated and other factors may be influencing the observed biological activity. Cellular uptake may be one of them. The synthesized PMIs can be named as head–tail PMIs where the hydrophobic nature of the head formed by the adamantane group and the perylene core facilitate transport through the cellular membrane and the hydrophilic chains (charged substituents, extended biotine and PEG chains) favor water solubility, prevent aggregation and enable H bonding. These features along with their emission properties are key for their cellular visualization. In fact, cells treated with 6 μM of the compounds under study were visualized by fluorescence microscopy revealing that all the complexes are successfully internalized by A549 cells within 4 h of exposition (Figure S56). Since **PMI6** is the most active compound, its subcellular distribution has been studied in human embryonic kidney cells (HEK293) by confocal microscopy. **PMI6** displays a red emission pattern mainly in the cytoplasmic region of cells (Fig. 7). Therefore, colocalization experiments were performed by immunostaining the cells with markers for Golgi and mitochondrion (Figs. S57and S58). **PMI6** shows a high degree of colocalization with the marker for mitochondria TOM20, and according to the Mander's correlation coefficients, tM1 (the proportion of TOM20 overlap by **PMI6**) is 0.86 and tM2 (the proportion of **PMI6** overlap by TOM20) is 0.66. Thus, this perylene monoimide derivative seems to highly accumulate in mitochondria.

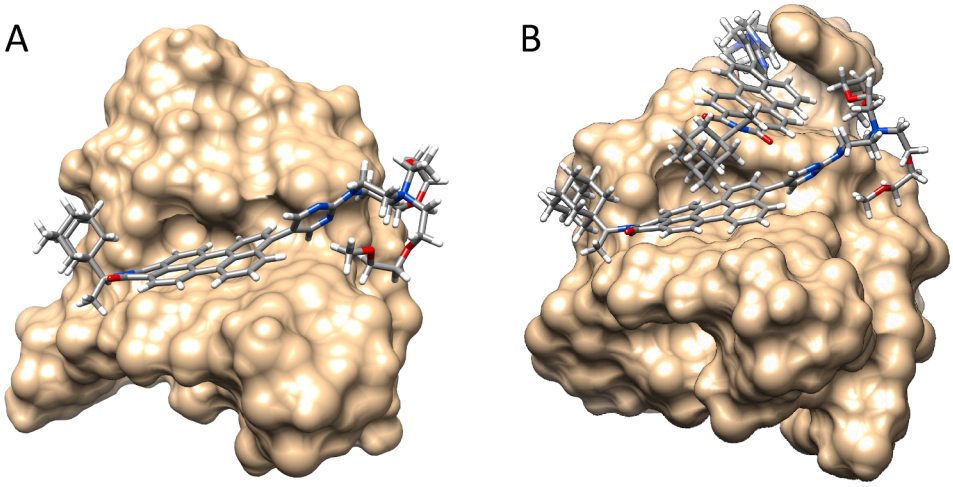

Fig. 6. Optimized structures of the **PMI6**/hTelo complex with **(A)** 1:1 and **(B)** 2:1 stoichiometry.

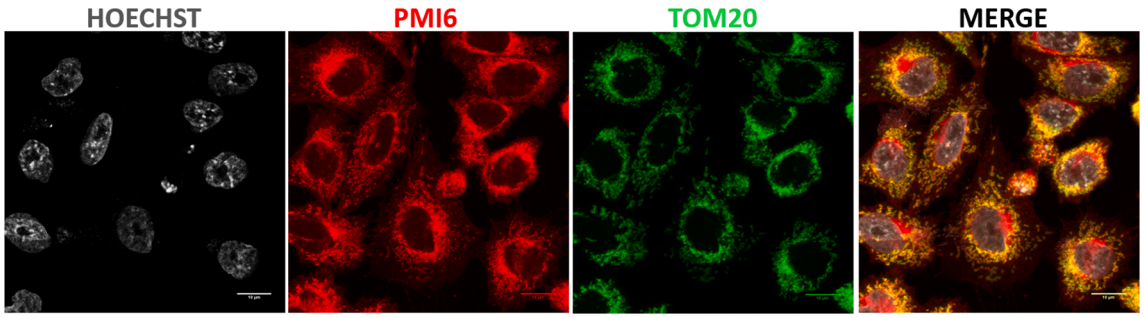

Fig. 7. Representative images of HEK293 cells treated with 3.5 μM of **PMI6**, a nucleus stain (Hoechst 33258) and the mitochondria antibody (TOM20). Scale bar: 10 μm

3. Conclusions

Six fluorescent perylenemonoimide derivatives were synthesized and fully characterized. Their ability to stabilize G-quadruplex structures was tested by the FRET melting assay. Among them, only **PMI1**, **PMI3** and **PMI6** induced thermal stabilizations of G4s. Interestingly, these three compounds exhibited different preferences, as **PM1** preferentially stabilized the parallel RNA G4 and the DNA human telomeric G4 (hTelo) which predominantly adopts a hybrid-type conformation, while **PMI3** preferred antiparallel G4s and **PMI6** preferred the human telomeric G4 (hTelo). Thus, for this series, a positive charge is required for the thermal stabilization of G-quadruplex structures. Also, the substitution of the pyrimidine by the pyridine moiety in these PMIs led to a change in thermal stabilization pattern between parallel and antiparallel G4s. The fluorescence of **PMI6** significantly increased in the presence of G4s but not with other DNA conformations (duplex, single strand or i-motifs). **PMI6** showed high affinity towards hTelo with at least two different binding processes that, according to QM/MM calculations corresponded to, first, the accommodation of a **PMI6** molecule in the groove of hTelo and then, another molecule of **PMI6** got bound to the terminal AT bases. Both processes were exothermic although the second one had an important entropic driven force. With respect to their biological activity, only three compounds, those bearing PEG chains at the *peri* position, **PMI2**, **PMI5** and **PMI6**, displayed antiproliferative activity, showing that the PEG chains seem to play a key role in the biological activity of this family of perylenemonoimides. Substitution of the pyrimidine by the pyridine moiety led to some enhancement of the antiproliferative activity. All the studied perylenemonoimide derivatives were able to enter the cells and could be visualized because of their orange emission. **PMI6** was the most cytotoxic compound in the series as well as the best G4 ligand and accumulated mainly in the mitochondria.

4. Experimental Section

Complete details of the synthesis and characterization of all compounds are given in the supporting information.

The dried human telomeric sequence, hTelo (d[AGGG(AGGGTT)$_3$]) was purchased for Thermo Fisher Scientific Inc. ctDNA was purchased for Sigma Aldrich as the lyophilized sodium salt. The double-labelled oligonucleotides have as the donor fluorophore in the 5′ end FAM (6-carboxyfluorescein) and as acceptor fluorophore TAMRA (6-carboxytetramethylrhodamine) in the 3′ end. These oligos used in the FRET Melting Assay, included an intramolecular duplex (F-dx-T: TATAGCTAT-hexaethyleneglycol-TATAGCTATA), six DNA G4s (F-hTelo-T: GGGTTAGGGTTAGGGTTAGGG, F-25Ceb-T: AGGGTGGGTGTAAGTGTGGGTGGGT, F-21CTA-T: GGGCTAGGGCTAGGGCTAGGG, F-myc-T: TGAGGGTGGGTAGGGTGGGTAA, F-Bom17-T: GGTTAGGTTAGGTTAGG and F-TBA-T: GGTTGGTGTGGTTGG) and a RNA G-quadruplex (F-21R-T: GGGUUAGGGUUAGGGUUAGGG). The DNA i-motif i-cmyc (TTACCCACCCTACCCACCCTCA), the single stranded DNA d17a (CCAGTTCGTAGTAACCC), the antiparallel DNA G-4 21CTA (GGGCTAGGGCTAGGGCTAGGG), the parallel DNA G-4c-myc (TGAGGGTGGGTAGGGTGGGTAA), the labelled oligonucleotides and the duplex used as competitor in competitions experiments, ds26 (CAATCGGATCGAATTCGATCCGATTG) were purchased from Eurogentec as dried samples and were prepared in doubly deionized water. Stock solutions of 100 μM double-labelled oligonucleotides and 500 μM of the unlabelled oligonucleotides were stored at −20 °C. For working solutions, stock solutions were diluted in annealing buffer consisting of 90 mM LiCl, 10 mM lithium cacodylate (LiCaC) and 10 mM KCl at pH = 7.2 except for the RNA G4, 21R that it is prepared in 99 mM LiCl, 10 mM LiCaC and 1 mM KCl at pH = 7.2. Then, for folding reactions, the solutions were heated at 90 °C during 5 min and then slowly cooled to room temperature, their concentration were spectrophotometrically determined at λ = 260 nm using the absorptivity coefficients provided by the manufacturer.

FRET Melting Assay was performed in a real time Polymerase Chain Reaction (7500 Fast Real Time PCR, Applied Biosystems) as previously described [20]. Briefly, samples containing 0.2 μM oligonucleotide in the absence and in the presence of different concentrations of PMI derivatives were prepared in 96-well plates and heated from 25 to 95 °C at 1 °C/min recording the emission of FAM and TAMRA. Thermal stabilization (ΔTm) was calculated as the difference between the mid-transition temperature of the oligonucleotide with and without the drug. In competition experiments, samples were prepared with 0.2 μM of F-hTelo-T, 5 and 10 μM of **PMI6** and ds26 as duplex competitor in an excess of 15 and 50 fold respecting hTelo. The experiments were conducted under the same conditions as the FRET melting assay previously described.

The acid dissociation constants (pKa) of **PMI3** was determined measuring the absorbance spectra in a dioso-array HP-8453 spectrophotometer (Agilent Technologies, Palo Alto, California as a function of pH. The pKa values were obtained plotting the absorbance at a fixed wavelength (λ) as a function of pH. The obtained data were analyzed according to the Henderson-Hasselbalch equation [55].

Time correlated single photon counting (TCSPC) measurements were carried out for the fluorescence decay of the **PMI6** in the absence and in the presence of two fold excess of G4s. The equipment used was FLS980 (Edinburgh Instruments). Photo excitation was made at 475 nm using an EPL 375 laser. The data were collected and analysed by FAST 3.4.0 software using the following equation: $F(t) = \sum \alpha_i \, e^{-(1/\tau I)}$, where, α_i and τ_i are the i^{th} preexponential factor and decay time of the excited species, respectively.

Fluorescence measurements were performed with a Shimadzu Corporation RF-5301PC spectrofluorometer (Duisburg, Germany) Titrations were carried out by adding increasing amounts of hTelo to the **PMI6** solution in a 1 cm path-length cells at 25 °C.

Isothermal titration calorimetry (ITC) experiments were performed at 25 °C using a Nano ITC (TA Instruments, Newcastle, USA). Prior to use, all solutions were degassed during 30 min in the degassing station (TA Instruments, Newcastle, USA) to avoid bubbles formation. Then, 25 injections of 2 μL of **PMI6** were injected into the calorimetric cell

containing the hTelo solution with a stirring speed of 250 rpm. Control experiments were carried out to determine the contribution of the heat of dilution of **PMI6** alone and rule out the presence of aggregation processes. The obtained thermograms were fitted with Nanoanalyze software by a "Multiple Binding Sites".

Circular dichroism (CD) spectra were recorded on a MOS-450 Biologic spectrometer (Claix, France), fitted with 1.0 cm path-length cells. Titrations were carried out at 25 °C by adding increasing amounts of the **PMI6** to the hTelo solution.

The geometry optimizations have been performed with the ORCA 4.2.0 software [56,57]. The structure of the telomere can be downloaded from RCSB website (PDB ID: 2hy9). The **PMI6** has been previously optimized through DFT theory using the hybrid functional B3LYP [58,59] and 6-31G** basis set [60] for all the atoms. The docking was done with the help of the AutoDock 4.0 software [61] using an efficient and durable algorithm, Lamarckian Genetic Algorithm (LGA) [62]. The two conformations with the lowest binding energy were further optimized using the GFN2-xTB method [63] as it is implemented in the ORCA 4.2.0 software. This method uses the basis def2-SVP [64]. Once optimized the complex hTelo-**PMI6** as an ensemble was used as "macromolecule" in AutoDock, adding a second molecule of **PM6** as ligand to study the interaction 1:2 followed by a further optimization using the GFN2-xTB method.

Cytotoxicity was studied by means of the CellTiter Non Radioactive Cell Proliferation Assay (Promega) in case of HeLa cells. Approximately 3×10^3 cells were cultured in EMEM (Eagle's Minimum Essential Medium medium) supplemented with supplemented with 1% of non-essential aminoacids and 10% Fetal Bovine Serum (FBS) in 96-well plates and incubated at 37 °C under a 5% CO_2 atmosphere. Cells were grown for 24 h and then treated with different concentrations of the PMI derivatives for 72 h. After the incubation period, the protocol described in technical specifications was followed. Absorbance was read at 570 nm in a microplate reader (Tecan Infinite M1000) and three replicates per dose were included. In A549 cells (cultured in Dulbecco's Modified Eagle's Medium (DMEM)), A2780 cells (cultured in RPMI-1640) and HEK293 (EMEM supplemented with supplemented with 1% of non-essential aminoacids), culture media were supplemented with 10% FBS and 1% amphotericin-penicillin–streptomycin solution. In both cell lines, the MTT Assays were performed with approximately 3×10^3 A549, 1×10^4 A2780 cells and HEK293 cells seeded in 96-well plates and incubated at 37 °C under a 5% CO_2 atmosphere. Cells were treated with different concentrations of the PMI derivatives under study during 72 h. Then, treatment was removed and cells were incubated with 100 μL of MTT (3-(4,5-dimethyltiazol-2-yl)-2,5-diphenyltetrazolium-bromide) (Sigma Aldrich) dissolved in culture medium (500 μg/ml). After 4 h, 100 μL of solubilizing solution (10% (w/v) SDS, 0.01 M HCl) were added to each well and incubated for other 18 h. At the end, absorbance at 590 nm was read in a microplate reader (Cytation 5 Cell Imaging Multi-Mode Reader - Biotek Instruments, USA). Four replicates per dose were included. The IC_{50} values were calculated from cell survival data of at least two independent experiments using GraphPadPrism Software Inc. version 6.01 (USA). In every case, cell death was confirmed by microscopy visualization of the treated cells.

For bioimaging experiments, A549 cells were seeded in appropriated 96-well plates at a density of 5×10^3 cells/well in 200 μL DMEM without phenol red and allow to adhere for 24 h at 37 °C and 5% CO_2. Then, cells were treated with 6 μM of the PMI derivatives and incubated at 37 °C under 5% CO_2 atmosphere for 4 h. Finally, cells were visualized in a Cytation 5 Cell Imaging Multi-Mode Reader (Biotek Instruments, USA) in bright field and orange fluorescence emission with a 20 × objective.

As to subcellular localization of **PMI6** by Leica SP5 confocal microscope system, HEK293 cells were incubated with 3.5 μM of **PMI6** for 1 h at 37 °C. Then the plates were washed once with PBS supplemented with 1 mM $CaCl_2$ and 1 mM $MgCl_2$, and then were fixed for 15 min at room temperature in 4% paraformaldehyde. A Leica SP5 confocal microscope system equipped with 6 different lasers was used for analyzing the spectrum of excitation and emission of the fluorescent probe in fixed cells. The fluorescent emission spectrum was assessed by using five different excitation wavelengths (λ_{EXC}): 488 nm, 496 nm, 514 nm, 561 nm and 633 nm. Although the maximum peak of emission was achieved with λ_{EXC} of 488 nm, dimmer emission was also detected with λ_{EXC} of 496 nm, 514 nm, 561 nm, but not with λ_{EXC} of 633 nm. Therefore, to study **PMI6** subcellular distribution, we combined subcellular-marker antibodies with Alexa-Fluor®633-conjugated secondary antibodies. GM130 (BD Biosciences #610822; 1:500) and Tom20 (SCBT#FL-145; 1:1000) were used as markers of Golgi apparatus and mitochondrion, respectively. To analyse co-localization, high resolution images (8192x8192 pixels) were acquired on a Leica SP5 confocal microscope. The whole cell area was outlined manually in each dual-labelled confocal image and then processed with the Coloc2 plugin of the Fiji version of the ImageJ image processing software. To calculate the co-localization between Tom20 and **PMI6**, Mander's coefficients with thresholds[65] and the associated Costes P-values[66] were obtained for every cell. A total of 21 cells from 3 different experiments were analyzed. All the coefficients were verified with the Costes statistical significance test.

Declaration of Competing Interest

The authors declared that there is no conflict of interest.

Acknowledgements

The financial support of "la Caixa" Foundation (LCF/PR/PR12/11070003), Ministerio de Ciencia, Innovación y Universidades-FEDER (RTI2018-102040-B-100), Junta de Castilla y León-FEDER (BU305P18 and BU263P18) is gratefully acknowledged. N.B. is grateful to Aurore Guédin of the ARNA Laboratory for technical support and also to the financial support of the José Castillejo Program by the Spanish Ministry of Education, Culture and Sports (JC2015-00403). A.H. was funded by a Juan de la Cierva fellowship (FJCI-2015-26175) from the Ministerio de Economía y Competitividad. This research has made use of the high-performance computing resources of the Castilla y León Supercomputing Center (SCAYLE, https://www.scayle.es), financed by FEDER (Fondo Europeo de Desarrollo Regional). Networking support of NECTAR COST Action CA18202 is fully acknowledged. This work was supported by the SYMBIT project (reg. no. CZ.02.1.01/0.0/0.0/15_003/0000477) financed by the ERDF.

Appendix A. Supplementary data

Supplementary data to this article can be found online at https://doi.org/10.1016/j.bioorg.2021.104660.

References

[1] R. Hänsel-Hertsch, M. Di Antonio, S. Balasubramanian, DNA G-quadruplexes in the human genome: Detection, functions and therapeutic potential, Nat. Rev. Mol. Cell Biol. 18 (2017) 279–284, https://doi.org/10.1038/nrm.2017.3.
[2] N. Maizels, G4 -associated human diseases, EMBO Rep. 16 (2015) 910–922.
[3] J.T. Davis, G-Quartets 40 Years Later: From 5′-GMP to Molecular Biology and Supramolecular Chemistry, Angew. Chemie Int. Ed. 43 (2004) 668–698, https://doi.org/10.1002/anie.200300589.
[4] T. Ou, Y. Lu, J. Tan, Z. Huang, K.-Y. Wong, L. Gu, G-Quadruplexes: Targets in Anticancer Drug Design, ChemMedChem 3 (2008) 690–713, https://doi.org/10.1002/cmdc.200700300.
[5] Q. Cao, Y. Li, E. Freisinger, P.Z. Qin, R.K.O. Sigel, Z.W. Mao, G-quadruplex DNA targeted metal complexes acting as potential anticancer drugs, Inorg. Chem. Front. 4 (2017) 10–32, https://doi.org/10.1039/c6qi00300a.
[6] Z.Y. Sun, X.N. Wang, S.Q. Cheng, X.X. Su, T.M. Ou, Developing novel G-quadruplex ligands: From interaction with nucleic acids to interfering with nucleic acid–protein interaction, Molecules 24 (2019), https://doi.org/10.3390/molecules24030396.
[7] S. Asamitsu, S. Obata, Z. Yu, T. Bando, H. Sugiyama, Recent progress of targeted G-quadruplex-preferred ligands toward cancer therapy, Molecules 24 (2019), https://doi.org/10.3390/molecules24030429.

[8] S. Neidle, Quadruplex nucleic acids as targets for anticancer therapeutics, Nat. Rev. Chem. 1 (2017) 1–10, https://doi.org/10.1038/s41570-017-0041.

[9] M.L. Bochman, K. Paeschke, V.A. Zakian, DNA secondary structures: stability and function of G-quadruplex structures, Nat. Rev. Genet. 13 (2012) 770–780, https://doi.org/10.1038/nrg3296.

[10] G. Miglietta, M. Russo, G. Capranico, G-quadruplex–R-loop interactions and the mechanism of anticancer G-quadruplex binders, Nucleic Acids Res. (2020) 1–16, https://doi.org/10.1093/nar/gkaa944.

[11] J. Carvalho, J.-L. Mergny, G.F. Salgado, J.A. Queiroz, C. Cruz, G-quadruplex, Friend or Foe: The Role of the G-quartet in Anticancer Strategies, Trends Mol. Med. 26 (2020) 848–861, https://doi.org/10.1016/j.molmed.2020.05.002.

[12] N. Saranathan, P. Vivekanandan, G-Quadruplexes: More Than Just a Kink in Microbial Genomes, Trends Microbiol. 27 (2019) 148–163, https://doi.org/10.1016/j.tim.2018.08.011.

[13] E. Ruggiero, S.N. Richter, Viral G-quadruplexes: New frontiers in virus pathogenesis and antiviral therapy, Annu. Rep. Med. Chem. 54 (2020) 101–131, https://doi.org/10.1016/bs.armc.2020.04.001.

[14] E. Ruggiero, S.N. Richter, Survey and summary G-quadruplexes and G-quadruplex ligands: Targets and tools in antiviral therapy, Nucleic Acids Res. 46 (2018) 3270–3283, https://doi.org/10.1093/nar/gky187.

[15] N. Panera, A.E. Tozzi, A. Alisi, The G-Quadruplex/Helicase World as a Potential Antiviral Approach Against COVID-19, Drugs. 80 (2020) 941–946, https://doi.org/10.1007/s40265-020-01321-z.

[16] M. Zuffo, F. Doria, S. Botti, G. Bergamaschi, M. Freccero, G-quadruplex fluorescence sensing by core-extended naphthalene diimides, Biochim. Biophys. Acta - Gen. Subj. 2017 (1861) 1303–1311, https://doi.org/10.1016/j.bbagen.2016.11.034.

[17] M.I. Umar, D. Ji, C.-Y. Chan, C.K. Kwok, G-Quadruplex-Based Fluorescent Turn-On Ligands and Aptamers: From Development to Applications, Molecules 24 (2019) 2416, https://doi.org/10.3390/molecules24132416.

[18] L. Rossetti, M. Franceschin, A. Bianco, G. Ortaggi, M. Savino, Perylene diimides with different side chains are selective in inducing different G-Quadruplex DNA structures and in inhibiting telomerase, Bioorg. Med. Chem. Lett. 12 (2002) 2527–2533, https://doi.org/10.1016/S0960-894X(02)00504-8.

[19] J.T. Kern, S.M. Kerwin, The aggregation and G-quadruplex DNA selectivity of charged 3,4,9,10-perylenetetracarboxylic acid diimides, Bioorg. Med. Chem. Lett. 12 (2002) 3395–3398, https://doi.org/10.1016/S0960-894X(02)00763-1.

[20] N. Busto, P. Calvo, J. Santolaya, J.M. Leal, A. Guédin, G. Barone, T. Torroba, J.-L. Mergny, B. García, Fishing for G-Quadruplexes in Solution with a Perylene Diimide Derivative Labeled with Biotins, Chem. - A Eur. J. 24 (2018) 11292–11296, https://doi.org/10.1002/chem.201802365.

[21] O.Y. Fedoroff, M. Salazar, H. Han, V.V. Chemeris, S.M. Kerwin, L.H. Hurley, NMR-based model of a telomerase-inhibiting compound bound to G- quadruplex DNA, Biochemistry 37 (1998) 12367–12374, https://doi.org/10.1021/bi981330n.

[22] S. Vasimalla, S. Sato, F. Takenaka, Y. Kurose, S. Takenaka, Cyclic perylene diimide: Selective ligand for tetraplex DNA binding over double stranded DNA, Bioorganic Med. Chem. 25 (2017) 6404–6411, https://doi.org/10.1016/j.bmc.2017.10.014.

[23] C. Pivetta, L. Lucatello, A. Paul Krapcho, B. Gatto, M. Palumbo, C. Sissi, Perylene side chains modulate G-quadruplex conformation in biologically relevant DNA sequences, Bioorg. Med. Chem. 16 (2008) 9331–9339, https://doi.org/10.1016/j.bmc.2008.08.068.

[24] M. Franceschin, A. Rizzo, V. Casagrande, E. Salvati, A. Alvino, A. Altieri, A. Ciammaichella, S. Iachettini, C. Leonetti, G. Ortaggi, M. Porru, A. Bianco, A. Biroccio, Aromatic Core Extension in the Series of N-Cyclic Bay-Substituted Perylene G-Quadruplex Ligands: Increased Telomere Damage Antitumor Activity, and Strong Selectivity for Neoplastic over Healthy Cells, ChemMedChem. 7 (2012) 2144–2154, https://doi.org/10.1002/cmdc.201200348.

[25] V. Casagrande, E. Salvati, A. Alvino, A. Bianco, A. Ciammaichella, C. D'Angelo, L. Ginnari-Satriani, A.M. Serrilli, S. Iachettini, C. Leonetti, S. Neidle, G. Ortaggi, M. Porru, A. Rizzo, M. Franceschin, A. Biroccio, N-cyclic bay-substituted perylene g-quadruplex ligands have selective antiproliferative effects on cancer cells and induce telomere damage, J. Med. Chem. 54 (2011) 1140–1156, https://doi.org/10.1021/jm1013665.

[26] M. Porru, P. Zizza, M. Franceschin, C. Leonetti, A. Biroccio, EMICORON: A multi-targeting G4 ligand with a promising preclinical profile, Biochim. Biophys. Acta - Gen. Subj. 2017 (1861) 1362–1370, https://doi.org/10.1016/j.bbagen.2016.11.010.

[27] T. Taka, K. Joonlasak, L. Huang, T. Randall Lee, S.W.T. Chang, W. Tuntiwechapikul, Down-regulation of the human VEGF gene expression by perylene monoimide derivatives, Bioorganic Med. Chem. Lett. 22 (2012) 518–522, https://doi.org/10.1016/j.bmcl.2011.10.089.

[28] T. Taka, L. Huang, A. Wongnoppavich, S.W. Tam-Chang, T.R. Lee, W. Tuntiwechapikul, Telomere shortening and cell senescence induced by perylene derivatives in A549 human lung cancer cells, Bioorganic Med. Chem. 21 (2013) 883–890, https://doi.org/10.1016/j.bmc.2012.12.020.

[29] N. Kaewtunjai, R. Summart, A. Wongnoppavich, B. Lojanapiwat, T.R. Lee, W. Tuntiwechapikul, Telomerase Inhibition, Telomere Shortening, and Cellular Uptake of the Perylene Derivatives PM2 and PIPER in Prostate Cancer Cells, Biol. Pharm. Bull. 42 (2019) 906–914, https://doi.org/10.1248/bpb.b18-00860.

[30] D. Görl, X. Zhang, F. Würthner, Molecular Assemblies of Perylene Bisimide Dyes in Water, Angew. Chemie Int. Ed. 51 (2012) 6328–6348, https://doi.org/10.1002/anie.201108690.

[31] M. Sun, K. Müllen, M. Yin, Water-soluble perylenediimides: Design concepts and biological applications, Chem. Soc. Rev. 45 (2016) 1513–1528, https://doi.org/10.1039/c5cs00754b.

[32] H. Liu, Y. Wang, C. Liu, H. Li, B. Gao, L. Zhang, F. Bo, Q. Bai, X. Ba, Fluorescent water-soluble probes based on dendritic PEG substituted perylene bisimides: Synthesis, photophysical properties, and live cell images, J. Mater. Chem. 22 (2012) 6176–6181, https://doi.org/10.1039/c2jm30168g.

[33] R. Buscaglia, M.C. Miller, W.L. Dean, R.D. Gray, A.N. Lane, J.O. Trent, J.B. Chaires, Polyethylene glycol binding alters human telomere G-quadruplex structure by conformational selection, Nucleic Acids Res. 41 (2013) 7934–7946, https://doi.org/10.1093/nar/gkt440.

[34] Z.F. Wang, T.C. Chang, Molecular engineering of G-quadruplex ligands based on solvent effect of polyethylene glycol, Nucleic Acids Res. 40 (2012) 8711–8720, https://doi.org/10.1093/nar/gks578.

[35] J. García-Calvo, J.A. Robson, T. Torroba, J.D.E.T. Wilton-Ely, Synthesis and Application of Ruthenium(II) Alkenyl Complexes with Perylene Fluorophores for the Detection of Toxic Vapours and Gases, Chem. – A Eur. J. 25 (2019) 14214–14222, https://doi.org/10.1002/chem.201903303.

[36] J. García-Calvo, P. Calvo-Gredilla, M. Ibáñez-Llorente, D.C. Romero, J.V. Cuevas, G. García-Herbosa, M. Avella, T. Torroba, Surface functionalized silica nanoparticles for the off–on fluorogenic detection of an improvised explosive, TATP, in a vapour flow, J. Mater. Chem. A 6 (2018) 4416–4423, https://doi.org/10.1039/C7TA10792G.

[37] J. García-Calvo, T. Torroba, V. Brañas-Fresnillo, G. Perdomo, I. Cózar-Castellano, Y.-H. Li, Y.-M. Legrand, M. Barboiu, Manipulation of Transmembrane Transport by Synthetic K+ Ionophore Depsipeptides and Its Implications in Glucose-Stimulated Insulin Secretion in β-Cells, Chem. – A Eur. J. 25 (2019) 9287–9294, https://doi.org/10.1002/chem.201901372.

[38] M. Ladinig, W. Leupin, M. Meuwly, M. Respondek, J. Wirz, V. Zoete, Protonation Equilibria ofHoechst 33258 in Aqueous Solution, Helv. Chim. Acta 88 (2005) 53–67, https://doi.org/10.1002/hlca.200490296.

[39] B. Prasad, R.N. Das, J. Jamroskovic, R. Kumar, M. Hedenström, N. Sabouri, E. Chorell, The Relation Between Position and Chemical Composition of Bis-Indole Substituents Determines their Interactions with G-Quadruplex DNA, Chem. - A Eur. J. (2020) 1–13, https://doi.org/10.1002/chem.202000579.

[40] D. Zhao, X. Dong, N. Jiang, D. Zhang, C. Liu, Selective recognition of parallel and anti-parallel thrombin-binding aptamer G-quadruplexes by different fluorescent dyes, Nucleic Acids Res. 42 (2014) 11612–11621, https://doi.org/10.1093/nar/gku833.

[41] F. Zhang, G. Li, F.-L. Lv, G.-B. Jiang, H.-X. Wang, M.-Q. Wang, S. Li, A far-red fluorescent probe for selective G-quadruplex DNA targeting, Tetrahedron Lett. 59 (2018) 3272–3278, https://doi.org/10.1016/j.tetlet.2018.07.037.

[42] P. Kumar, R. Barthwal, Structural and biophysical insight into dual site binding of the protoberberine alkaloid palmatine to parallel G-quadruplex DNA using NMR, fluorescence and Circular Dichroism spectroscopy, Biochimie 147 (2018) 153–169, https://doi.org/10.1016/j.biochi.2018.02.002.

[43] S.-B. Chen, W.-B. Wu, M.-H. Hu, T.-M. Ou, L.-Q. Gu, J.-H. Tan, Z.-S. Huang, Discovery of a new fluorescent light-up probe specific to parallel G-quadruplexes, Chem. Commun. 50 (2014) 12173–12176, https://doi.org/10.1039/C4CC05394J.

[44] J. Mohanty, N. Barooah, V. Dhamodharan, S. Harikrishna, P.I. Pradeepkumar, A. C. Bhasikuttan, Thioflavin T as an Efficient Inducer and Selective Fluorescent Sensor for the Human Telomeric G-Quadruplex DNA, J. Am. Chem. Soc. 135 (2013) 367–376, https://doi.org/10.1021/ja309588h.

[45] Y. Kataoka, H. Fujita, Y. Kasahara, T. Yoshihara, S. Tobita, M. Kuwahara, Minimal Thioflavin T Modifications Improve Visual Discrimination of Guanine-Quadruplex Topologies and Alter Compound-Induced Topological Structures, Anal. Chem. 86 (2014) 12078–12084, https://doi.org/10.1021/ac5028325.

[46] L.-L. Li, H.-R. Xu, K. Li, Q. Yang, S.-L. Pan, X.-Q. Yu, Mitochondrial G-quadruplex targeting probe with near-infrared fluorescence emission, Sensors Actuators B Chem. 286 (2019) 575–582, https://doi.org/10.1016/j.snb.2019.01.169.

[47] W.-C. Huang, T.-Y. Tseng, Y.-T. Chen, C.-C. Chang, Z.-F. Wang, C.-L. Wang, T.-N. Hsu, P.-T. Li, C.-T. Chen, J.-J. Lin, P.-J. Lou, T.-C. Chang, Direct evidence of mitochondrial G-quadruplex DNA by using fluorescent anti-cancer agents, Nucleic Acids Res. (2015) gkv1061, https://doi.org/10.1093/nar/gkv1061.

[48] T.-Y. Tseng, I.-T. Chu, S.-J. Lin, J. Li, T.-C. Chang, Binding of Small Molecules to G-quadruplex DNA in Cells Revealed by Fluorescence Lifetime Imaging Microscopy of o-BMVC Foci, Molecules 24 (2018) 35, https://doi.org/10.3390/molecules24010035.

[49] L.-Y. Liu, W. Liu, K.-N. Wang, B.-C. Zhu, X.-Y. Xia, L.-N. Ji, Z.-W. Mao, Content Detection of G-Quadruplex DNA in Live Cells Based on Photon Counts and Complex Structures, Angew. Chemie. (2020), https://doi.org/10.1002/ange.202002422 ange.202002422.

[50] A. Łęczkowska, J. Gonzalez-Garcia, C. Perez-Arnaiz, B. Garcia, A.J.P. White, R. Vilar, Binding Studies of Metal-Salphen and Metal-Bipyridine Complexes towards G-Quadruplex DNA, Chem. - A Eur. J. 24 (2018) 11785–11794, https://doi.org/10.1002/chem.201802248.

[51] V.S. Stafford, K. Suntharalingam, A. Shivalingam, A.J.P. White, D.J. Mann, R. Vilar, Syntheses of polypyridyl metal complexes and studies of their interaction with quadruplex DNA, Dalt. Trans. 44 (2015) 3686–3700, https://doi.org/10.1039/c4dt02910k.

[52] Y.X. Xiong, Z.S. Huang, J.H. Tan, Targeting G-quadruplex nucleic acids with heterocyclic alkaloids and their derivatives, Eur. J. Med. Chem. 97 (2015) 538–551, https://doi.org/10.1016/j.ejmech.2014.11.021.

[53] L.H. Hurley, R.T. Wheelhouse, D. Sun, S.M. Kerwin, M. Salazar, O.Y. Fedoroff, F. X. Han, H. Han, E. Izbicka, D.D. Von Hoff, G-quadruplexes as targets for drug design, Pharmacol. Ther. 85 (2000) 141–158, https://doi.org/10.1016/S0163-7258(99)00068-6.

[54] O.Y. Fedoroff, M. Salazar, H. Han, V.V. Chemeris, S.M. Kerwin, L.H. Hurley, NMR-Based Model of a Telomerase-Inhibiting Compound Bound to G-Quadruplex DNA †, Biochemistry 37 (1998) 12367–12374, https://doi.org/10.1021/bi981330n.
[55] H.N. Po, N.M. Senozan, The Henderson-Hasselbalch Equation: Its History and Limitations, J. Chem. Educ. 78 (2001) 1499, https://doi.org/10.1021/ed078p1499.
[56] F. Neese, The ORCA program system, WIREs Comput. Mol. Sci. 2 (2012) 73–78, https://doi.org/10.1002/wcms.81.
[57] F. Neese, Software update: the ORCA program system, version 4.0, WIREs Comput. Mol. Sci. 8 (2018), https://doi.org/10.1002/wcms.1327.
[58] A.D. Becke, Density-functional thermochemistry. III. The role of exact exchange, J. Chem. Phys. 98 (1993) 5648–5652, https://doi.org/10.1063/1.464913.
[59] C. Lee, W. Yang, R.G. Parr, Development of the Colle-Salvetti correlation-energy formula into a functional of the electron density, Phys. Rev. B. 37 (1988) 785–789, https://doi.org/10.1103/PhysRevB.37.785.
[60] P.C. Hariharan, J.A. Pople, The influence of polarization functions on molecular orbital hydrogenation energies, Theor. Chim. Acta 28 (1973) 213–222, https://doi.org/10.1007/BF00533485.
[61] G.M. Morris, D.S. Goodsell, R.S. Halliday, R. Huey, W.E. Hart, R.K. Belew, A. J. Olson, Automated docking using a Lamarckian genetic algorithm and an empirical binding free energy function, J. Comput. Chem. 19 (1998) 1639–1662, https://doi.org/10.1002/(SICI)1096-987X(19981115)19:14<1639::AID-JCC10>3.0.CO;2-B.
[62] G.M. Morris, R. Huey, W. Lindstrom, M.F. Sanner, R.K. Belew, D.S. Goodsell, A. J. Olson, AutoDock4 and AutoDockTools4: Automated docking with selective receptor flexibility, J. Comput. Chem. 30 (2009) 2785–2791, https://doi.org/10.1002/jcc.21256.
[63] C. Bannwarth, S. Ehlert, S. Grimme, GFN2-xTB—An Accurate and Broadly Parametrized Self-Consistent Tight-Binding Quantum Chemical Method with Multipole Electrostatics and Density-Dependent Dispersion Contributions, J. Chem. Theory Comput. 15 (2019) 1652–1671, https://doi.org/10.1021/acs.jctc.8b01176.
[64] F. Weigend, R. Ahlrichs, Balanced basis sets of split valence, triple zeta valence and quadruple zeta valence quality for H to Rn: Design and assessment of accuracy, PCCP 7 (2005) 3297–3305, https://doi.org/10.1039/b508541a.
[65] E.M.M. Manders, F.J. Verbeek, J.A. Aten, Measurement of co-localization of objects in dual-colour confocal images, J. Microsc. 169 (1993) 375–382, https://doi.org/10.1111/j.1365-2818.1993.tb03313.x.
[66] S.V. Costes, D. Daelemans, E.H. Cho, Z. Dobbin, G. Pavlakis, S. Lockett, Automatic and Quantitative Measurement of Protein-Protein Colocalization in Live Cells, Biophys. J. 86 (2004) 3993–4003, https://doi.org/10.1529/biophysj.103.038422.